catalysts

MDPI

Article

# Room-Temperature Nitrophenol Reduction over Ag–$CeO_2$ Catalysts: The Role of Catalyst Preparation Method

**Mariia Chernykh [1], Natalia Mikheeva [1], Vladimir Zaikovskii [2,3], Mikhail Salaev [1], Leonarda F. Liotta [4] and Grigory Mamontov [1,*]**

1 Laboratory of Catalytic Research, Tomsk State University, 634050 Tomsk, Russia; msadlivskaya@mail.ru (M.C.); natlitv93@yandex.ru (N.M.); mihan555@yandex.ru (M.S.)
2 Laboratory of Structural Research Methods, Boreskov Institute of Catalysis SB RAS, 630090 Novosibirsk, Russia; viz@catalysis.ru
3 Department of Physics, Novosibirsk State University, 630090 Novosibirsk, Russia
4 Institute for the Study of Nanostructured Materials (ISMN), (Italian) National Research Council (CNR), Via Ugo La Malfa 153, 90146 Palermo, Italy; leonardafrancesca.liotta@cnr.it
* Correspondence: GrigoriyMamontov@mail.ru; Tel.: +7-913-883-5124

Received: 27 April 2020; Accepted: 20 May 2020; Published: 21 May 2020


**Abstract:** Ag–$CeO_2$ catalysts (20 mol % Ag) were synthesized using different techniques (co-precipitation, impregnation, and impregnation of pre-reduced ceria), characterized by XRD, $N_2$ sorption, TEM, $H_2$-TPR methods, and probed in room-temperature p-nitrophenol reduction into p-aminophenol in aqueous solution at atmospheric pressure. The catalyst preparation method was found to determine the textural characteristics, the oxidation state and distribution of silver and, hence, the catalytic activity in the p-nitrophenol reduction. The impregnation technique was the most favorable for the formation over the ceria surface of highly dispersed silver species that are active in the p-nitrophenol reduction (the first-order rate constant k = 0.656 $min^{-1}$).

**Keywords:** Ag–$CeO_2$ catalysts; nitrophenol reduction; mild conditions; metal–support interaction; catalysts preparation

## 1. Introduction

Catalytic reduction of nitrocompounds is actively used in the cleaning of the environment from nitroarenes, including explosive nitrocompounds [1], and in industrial manufacturing of amino compounds [2]. Toxic properties of nitroarenes are presented in many publications [3,4]. There are several methods to reduce nitrocompounds, namely, chemical reduction [1], biological reduction [5], photocatalytic degradation [6], electrochemical methods [7], etc. However, the transformation of the nitrogroup into an aminogroup by catalytic hydrogenation is the most widely used, since it has low energy-intensiveness and does not use harmful organic solvents [8]. The liquid-phase reduction of nitroarenes has a significant environmental impact on wastewater purification and push for the decision by using new sorbents [9], catalysts and technical solutions [10].

Despite the fact that there have been many studies of the catalytic hydrogenation of nitroaromatics, many catalysts do not meet the requirements for practical use, and there are still several challenges:

1) Due to the high cost of Pd and Pt catalysts, the development of catalysts without Pt-group metals, such as Au-based ones, is required.

2) Carrying out selective hydrogenation with the preservation of other functional groups. In addition, controlling the degree of recovery of the nitrogroup to produce a fully hydrogenated amino group is of great interest.

3) Obtaining a material with a high catalytic performance, since the selectivity increase often leads to a decrease in activity.

Therefore, the elaboration of active, selective, and environmentally benign catalysts to synthesize amines is essential.

Catalysts based on noble metals [11] are used to reduce nitrocompounds under mild conditions. Contrary to other noble metals, silver is a cheaper raw material that possesses high chemical activity [12–14]. Recently, Liao et al. [15] overviewed the features of p-nitrophenol reduction over Ag catalysts. It was shown that several factors determine the catalytic properties of the deposited Ag particles: dispersion (particle size), particle shape, pretreatment conditions, the nature of the precursor, support, etc.

In our previous work, we showed that for $Ag/CeO_2$, the metal–support interaction contributes to enhancing the catalytic activity in CO and soot oxidation [16]. For $CeO_2$ support, in addition to its unique redox properties, the strong metal–support interaction (SMSI) and electronic metal–support interaction (EMSI) are characteristic phenomena having an impact on the following oxidation processes: electro-oxidation of methanol [17], CO oxidation [18], hydrogenation of quinolones [19], photocatalytic reactions [20]. The role of the features of the metal–support interaction in reduction processes is poorly discussed in the literature [21], especially for $Ag/CeO_2$ catalysts [22,23].

In the present work by varying some experimental conditions with respect to the $Ag/CeO_2$ series previously reported [16], we have synthesized three $Ag–CeO_2$ catalysts with relatively high Ag loading (20 mol. % corresponding to ~13.6 wt. %). Different techniques have been used in order to control Ag oxidation state and particle size distribution, as well as $Ag–CeO_2$ interfacial interaction. Depending on the preparation method, the catalysts were labeled as follows: $Ag–CeO_2$ (by co-precipitation method), $Ag/CeO_2$ (impregnation of the as-prepared ceria) and $Ag/CeO_{2(red)}$ (impregnation of pre-reduced ceria).

The p-nitrophenol reduction into p-aminophenol in aqueous media with $NaBH_4$ under mild conditions (room temperature, atmospheric pressure) was studied over the prepared $Ag–CeO_2$ catalysts.

## 2. Results

### 2.1. Result of $N_2$ Sorption

The porous structures of the samples were studied with low-temperature $N_2$ adsorption. The adsorption–desorption isotherms of ceria are characterized by the hysteresis loop in the range of relative pressures of 0.75–1.0 (Figure 1a) indicating a broad distribution of mesopores in the structure [24]. For silver-containing catalysts, the hysteresis loops are smaller and shifted to relative pressures of 0.9–1.0, indicating the decreased amount of mesopores and the formation of wide pores or interparticle voids. The pore size distribution images (Figure 1b) show that $CeO_2$ has mesopores and macropores with widths in the range of ~5–100 nm and a maximum distribution at 13 nm. The specific surface ($S_{BET}$) for $CeO_2$ sample is 30 $m^2/g$ (Table 1).

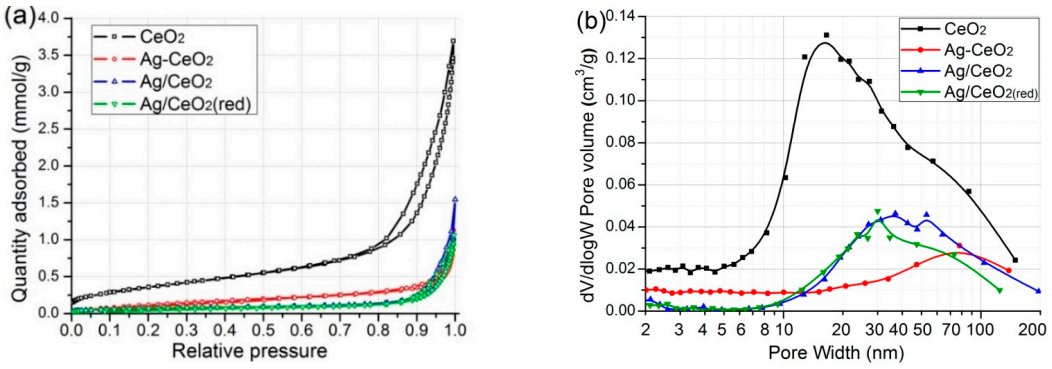


**Figure 1.** The isotherms of $N_2$ adsorption-desorption (**a**) and the corresponding pore size distributions (BJH-Desorption method) (**b**) for $CeO_2$ and catalysts.

**Table 1.** Textural characteristics of the Ag catalysts and $CeO_2$ support.

| Sample | $S_{BET}$ ($m^2$/g) | $V_{pore}$ ($cm^3$/g) | $D_{pore}$ (nm) * |
|---|---|---|---|
| $CeO_2$ | 30.4 | 0.128 | 13 |
| Ag–$CeO_2$ | 11.9 | 0.039 | - |
| Ag/$CeO_2$ | 5.6 | 0.054 | 27 |
| Ag/$CeO_2$ (red) | 5.6 | 0.037 | 27 |

* Pore width at the maximum of distribution curve (dV/dW pore volume vs pore width).

As results from the shape of isotherms and pore size distribution (Figure 1) and according to the values listed in Table 1, the textural properties of ceria were strongly modified upon introduction of silver, and the changes are a function of the catalyst preparation method. The Ag–$CeO_2$ catalyst prepared by co-precipitation possesses a specific surface of ~12 $m^2$/g and a pore volume of 0.039 $cm^3$/g. The contribution of pores of 10–100 nm is negligible (Figure 1b). The noticeable change of the porous structure of such Ag–$CeO_2$ sample as compared to $CeO_2$ may be due to the $Ag^+$–$Ce^{3+}$ redox reaction during the co-precipitation in alkaline condition [25]:

$$[Ag(NH_3)_2]OH + Ce(OH)_3 \rightarrow Ag + CeO_2 + 2\,NH_3{\cdot}H_2O \quad (1)$$

The Ag/$CeO_2$(red) and Ag/$CeO_2$ catalysts prepared by impregnation techniques have surface area as low as ~6 $m^2$/g (Table 1) and are characterized by 10–100-nm pores. The comparison of the porous structure of these catalysts with the pattern of $CeO_2$ support allows the conclusion that silver is predominantly localized in the pores with sizes below 20 nm, leading to a considerable decrease of both $S_{BET}$ and $V_{pore}$ values and to an increase in the average pore size distribution.

Based on the data reported so far, it emerges that the catalyst preparation method (co-precipitation or impregnation) affects their textural properties. The redox reaction between $Ce^{3+}$ and $Ag^+$ ions causes the decrease of $S_{BET}$ and the suppression of mesopores in the range of ~10–100 nm. Impregnation with silver leads to significant changes in the ceria porous structure, the decreased values of specific surface and pore volume are likely due to filling of the support pores by a relatively high amount of silver nanoparticles (13.6 wt. %), as well as to the second calcination treatment at 500 °C of the catalyst. The reductive pre-treatment of ceria support followed by the redox reaction of $Ag^+$ with the surface $Ce^{3+}$ species in the impregnating solution does not influence the textural characteristics.

### *2.2. XRD*

Figure 2 shows the XRD patterns for the obtained materials; in Table 2, the structural parameters are listed. Reflections of cubic $CeO_2$ are observed for all samples. In Figure 2b the enlarged region of the $CeO_2$ (111) peak at ~28.6° 2θ is displayed. The peak for the ceria support is not symmetric with an evident shoulder at slightly lower 2θ value that may indicate the defectiveness of ceria particles and high concentration of $Ce^{3+}$ ions [26,27]. This finding is in agreement with the precipitation conditions used in the present work as reported by Yamazaki et al. [25] to obtain a core–shell structure. The fast addition of ammonia solution to a small volume of water containing $Ce(NO_3)_3{\cdot}6H_2O$ led to the precipitation of highly defective ceria ($d_{(111)}$ = 3.131 Å) with small crystallite size, 8.8 nm, see Table 2). Co-precipitation of $AgNO_3$ and $Ce(NO_3)_3{\cdot}6H_2O$ in the same conditions as for the bare support, produced a well-crystalline ceria structure ($d_{(111)}$ = 3.121 Å). The size of ceria crystallites for the Ag–$CeO_2$ sample is 16.7 nm, which is significantly higher than for $CeO_2$ oxide, and may be a result of the abovementioned redox reaction that occurred during the co-precipitation. Thus, a significant agglomeration and growth of ceria may happen in the case of co-precipitation with the silver precursor.

Sintering of ceria particles also occurs for both Ag/$CeO_2$ and Ag/$CeO_2$(red) catalysts, and this was attributed to the reduction of the ceria support and successive calcination treatment. The observed growth of ceria crystal sizes correlates with the decreased $S_{BET}$ and pore volumes (Table 1) observed

for all silver catalysts in comparison with $CeO_2$. The $d_{(111)}CeO_2$ values for catalysts prepared by impregnation are close to that for the $CeO_2$ support.

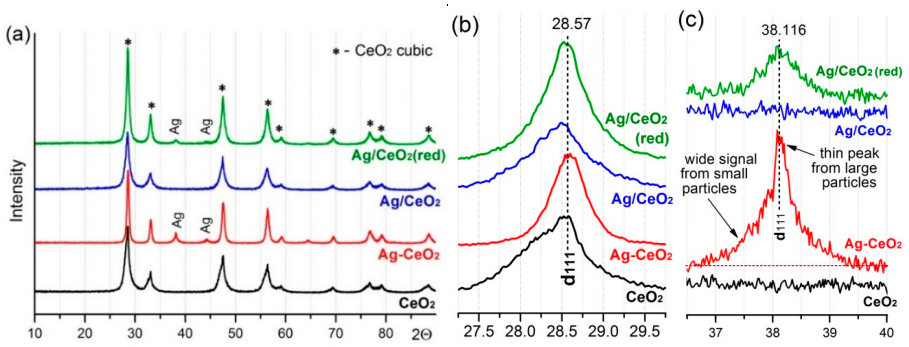


**Figure 2.** The powder XRD patterns for catalysts: panoramic spectrum (**a**), the detailed peaks of $CeO_2$ (111) (**b**) and Ag (111) (**c**).

**Table 2.** Structural parameters of the Ag catalysts and $CeO_2$ support.

| Sample | $d_{(111)CeO2}$ (Å) | $D_{CeO2}$ (nm) [a] | $d_{(111)Ag}$ (Å) | $D_{Ag}$ (nm) [a] |
|---|---|---|---|---|
| $CeO_2$ | 3.131 | 8.8 ± 1.0 | - | - |
| Ag–$CeO_2$ | 3.121 | 16.7 ± 1.8 | 2.361 | 17.0 ± 1.1 |
| Ag/$CeO_2$ | 3.130 | 9.9 ± 1.3 | - | - |
| Ag/$CeO_2$ (red) | 3.126 | 14.1 ±1.5 | 2.362 | 12.3 ± 0.7 |
| ICSD * reference files [b] | 3.121 | - | 2.359 | - |

[a] D (nm) particle size calculated by Scherrer equation, * Inorganic Crystal Structure Database, [b] FIZ Karlsruhe.

The reflections at ~38°, 44°, 65° 2θ, well detectable for Ag/$CeO_2$(red) and Ag-$CeO_2$ catalysts (see Figure 2c), correspond to metallic silver phase. The formation of $Ag^0$ may be a result of the redox reaction during the impregnation of the pre-reduced ceria and co-precipitation. For the co-precipitated Ag–$CeO_2$ sample, metallic silver crystallites with the sizes of up to 17 nm are formed (Table 2). The shape of the Ag peak for such a catalyst may indicate the presence of silver particles (crystallites) with different sizes, namely, the broadening could be due to small silver particles (below 5 nm, see HR-TEM), while the thin peak corresponds to relatively large particles. Particles of metallic silver with the size equal to 12 nm were found for Ag/$CeO_2$ (red), but in this case, too, the presence of smaller particles cannot be excluded, as confirmed by HR-TEM.

The absence of reflections of metallic Ag in the XRD pattern of Ag/$CeO_2$ may be due to its distribution predominantly in oxidative state and/or in highly dispersed species (less than 3 nm) that are below the detection limit of the XRD technique.

### *2.3. TEM Studies*

The high-resolution transmission electron microscopy was employed to study the structure of the obtained samples. Figure 3 shows the structure of the Ag–$CeO_2$ catalyst prepared by co-precipitation. Spherical aggregates with a diameter of ~400 nm are formed as a result of co-precipitation of silver and ceria nitrate accompanied by the redox reaction between $Ag^+$ and $Ce^{3+}$. The formation of similar Ag–$CeO_2$ agglomerates with a diameter of 200 nm was observed in Ref. [25] when silver and ceria precursors were co-precipitated, while the Ag loading was 39 wt. % and the core–shell structure was formed because of the agglomeration of $CeO_2$ particles around Ag cores (~50 nm). In our case, the Ag loading was much lower, ~13.6 wt. %, and silver cores were not formed. TEM images (Figure 3c,d) show that the catalyst contains aggregated particles with sizes of 5–20 nm. The measured interplanar distances correspond to metallic silver ($d_{111}$ = 2.3 Å) and ceria ($d_{111}$ = 3.1 Å) structures.

In Figure 4, the HR TEM images for the catalysts prepared by impregnation are displayed. The samples appear as aggregated ceria particles with sizes of ~10 nm, which is in line with the XRD

results. Small silver particles with a diameter of up to 5 nm are formed in the case of $Ag/CeO_2$ catalyst. This explains the absence of Ag-related reflexes in the XRD patterns because of the small sizes of Ag particles. Additionally, some metallic silver particles may be formed immediately during the TEM studies because of the instability of silver oxide species under vacuum and the action of the electron beam. The same distribution of Ag nanoparticles takes place for the $Ag/CeO_2$(red) catalysts (Figure 4c,d).

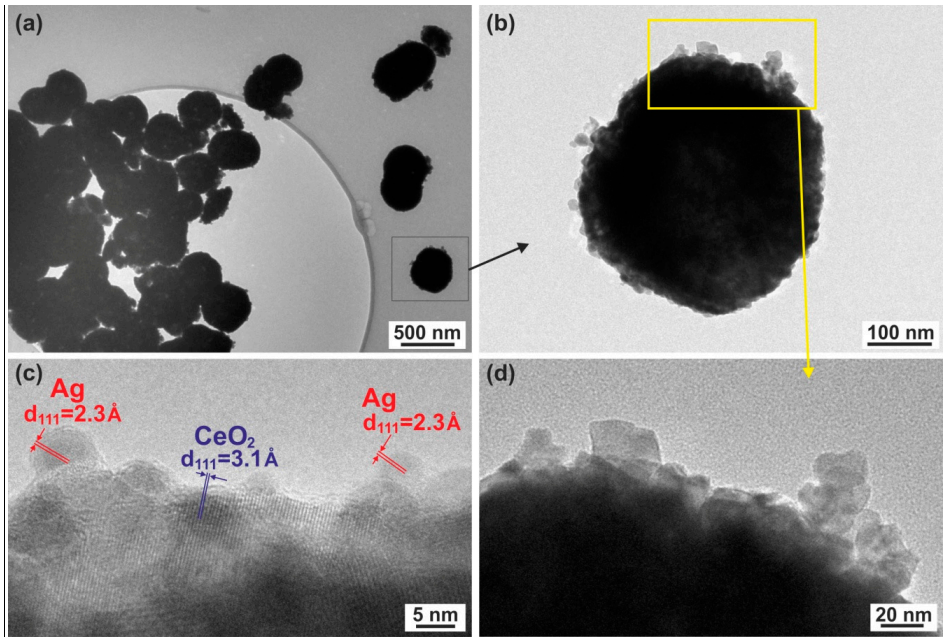


**Figure 3.** TEM (**a**,**b**,**d**) and HR-TEM (**c**) images of $Ag–CeO_2$ catalyst.

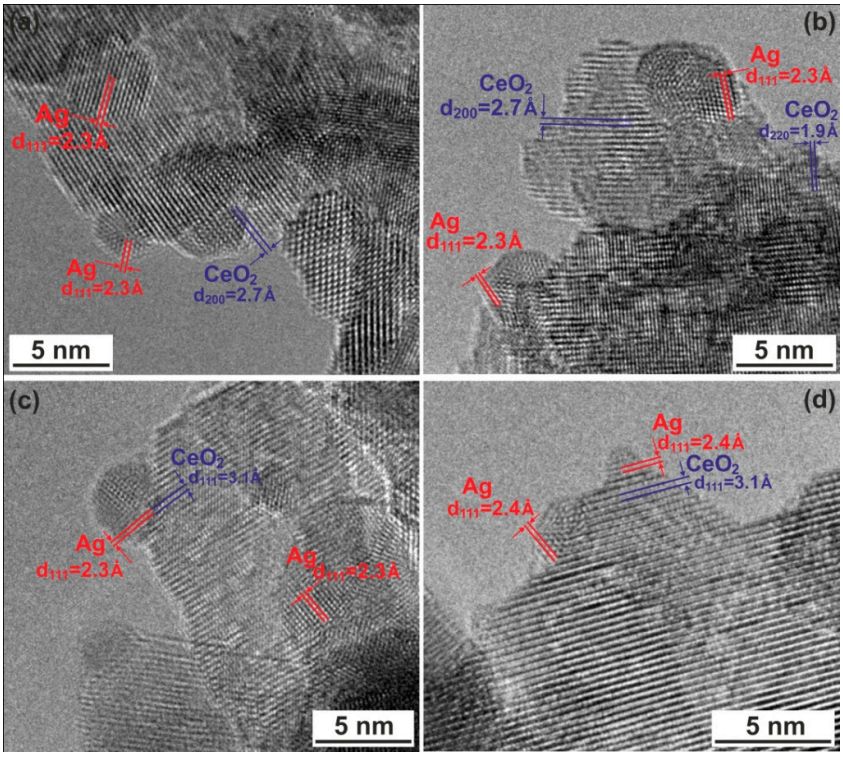


**Figure 4.** The HR TEM images for $Ag/CeO_2$ (**a**,**b**) and $Ag/CeO_2$(red) (**c**,**d**) catalysts.

### 2.4. $H_2$-TPR

The reduction properties of the prepared materials were studied by temperature-programmed reduction technique by using 10 vol. % $H_2$/Ar. Figure 5a shows the $H_2$-TPR profiles for all samples. Two temperature regions characterize the $CeO_2$ reduction: the reduction of bulk ceria occurs at 750–900 °C, while the peak at 300–600 °C corresponds to the ceria surface reduction [28]. For the Ag-containing samples, additional low-temperature hydrogen consumption features are observed. The peak at 130 °C may be assigned to $Ag_2O$ reduction [29], the peak at 150–250 °C was connected with the reduction of surface ceria in the presence of silver [30]. The hydrogen consumption at 70–250 °C may also be attributed to the reduction of mixed Ag-Ce oxide species or to reduction of the species at the Ag–$CeO_2$ interface [31].

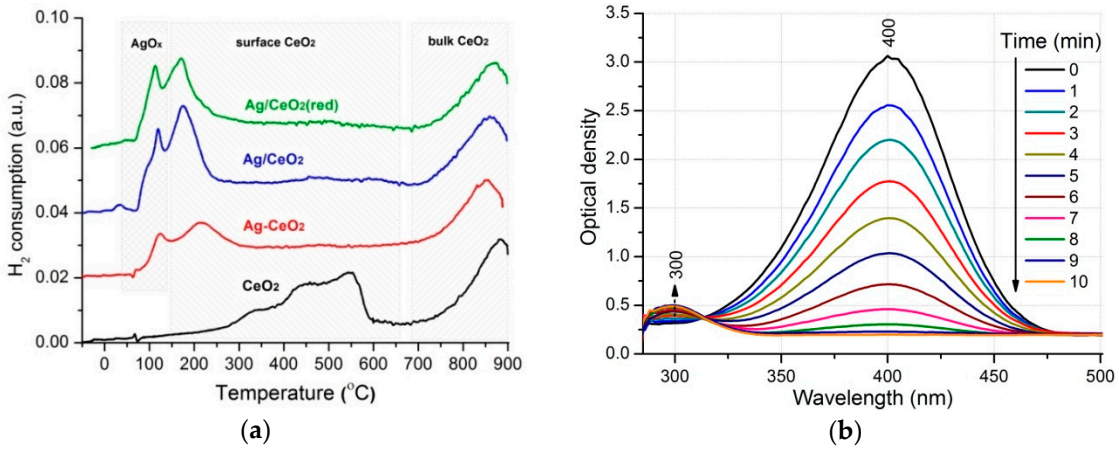


**Figure 5.** The $H_2$-TPR profiles for $CeO_2$ and catalysts (**a**), and UV-vis spectra during the reduction of p-nitrophenol over Ag-$CeO_2$ catalyst (**b**).

The TPR profiles for the catalysts show that the peak of $CeO_2$ surface reduction is significantly shifted from 300–600 °C ($CeO_2$ sample) to ~100–250 °C, which is caused by the Ag–$CeO_2$ interfacial interaction. Thus, cooperation of the active species of silver and $CeO_2$ is expected in the oxidative or reductive catalytic processes [23]. Since the intensities of the $H_2$ consumption peaks at 70–250 °C are higher for Ag/$CeO_2$(red) and Ag/$CeO_2$ catalysts compared to the one for Ag–$CeO_2$ catalyst prepared by the co-precipitation, this may be a result of both more homogeneous distribution of Ag particles on ceria support surface and smaller sizes of silver particles according to the data of TEM and XRD characterizations.

### 2.5. Catalytic Properties

The catalytic properties of the synthesized catalysts were investigated in p-nitrophenol reduction into p-aminophenol at ambient conditions using the $NaBH_4$ as a reductive agent. Figure 5b shows the UV-Vis spectra of the aqueous solution during the reduction of n-nitrophenol over the Ag-$CeO_2$ catalyst. The absorption band at 400 nm is typical for the nitrophenolate ion [32], and the one at ~300 nm corresponds to p-aminophenol. The intensity of the former band decreases indicating the p-nitrophenol conversion in the presence of the catalyst and $NaBH_4$. Total conversion is achieved for 10 min. At the same time, the intensity of the latter absorption band increases that indicates an increase in the concentration of aminophenol in the solution. Moreover, during the whole reaction, the color of the reaction mixture changes from yellow to colorless.

Figure 6a shows the changes of p-nitrophenol concentration with time of stirring of the aqueous solution with $NaBH_4$, with or without the catalyst. It can be seen that there is no reaction without the catalysts for 30 min. $CeO_2$ weakly catalyzes the reaction, and the p-nitrophenol conversion of ~20% ($C/C_0$ = 0.8) is achieved within 30 min. The reaction rate over Ag-containing catalysts is significantly

higher. Thus, the time of complete conversion of p-nitrophenol over the Ag–$CeO_2$ catalyst is ~10 min, while those for Ag/$CeO_2$ and Ag/$CeO_2$(red) catalysts are ~4 and ~8 min, respectively.

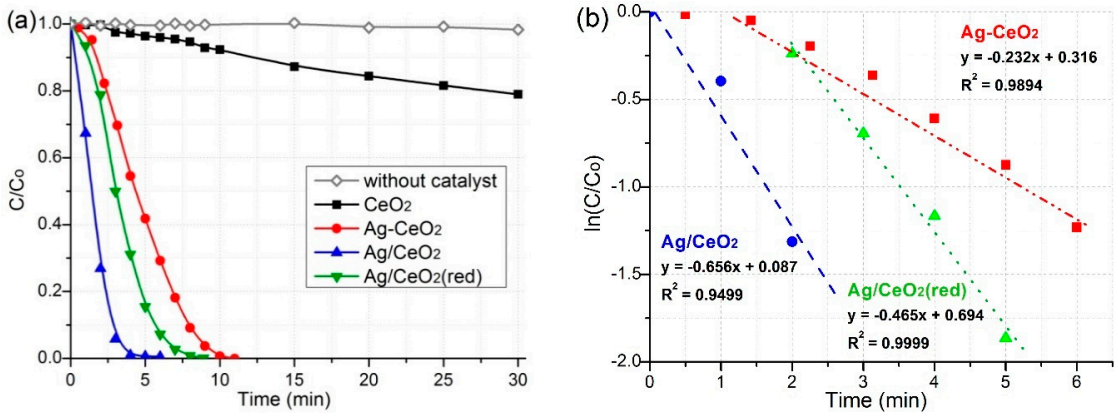


**Figure 6.** The dependences of p-nitrophenol concentration on time for different catalysts (**a**) and corresponding linearization of kinetic data in pseudo-first order coordinates (**b**).

The mechanism of the catalytic reduction of nitroarenes with $NaBH_4$ can be considered within the framework of the Langmuir-Hinshelwood theory: borohydride ions interact with the catalyst surface to produce adsorbed H atoms [33]. Simultaneously, the molecules of p-nitrophenol are adsorbed on the surface of Ag nanoparticles. Assuming that both steps (the diffusion of 4-nitrophenol from the volume of the solution to the surface of the catalyst and its adsorption on the surface of Ag nanoparticles) are rapid, the reduction of the adsorbed 4-nitrophenol by hydrogen atoms activated on the catalyst surface comprises the rate-determining step. Since the excess of $NaBH_4$ toward 4-nitrophenol was used, the activated hydrogen on the catalyst surface can be assumed constant. Consequently, this process can be considered a pseudo-first order reaction [34,35] and a linear dependence of the $\ln(C/C_0)$ versus time was found (Figure 6b). The reaction rate constants were calculated based on the slope constants of the straight-line equations and are listed in Table 3. The highest rate constant (k) is observed for Ag/$CeO_2$ catalyst. The lowest k value belongs to the Ag–$CeO_2$ catalyst. Table 3 compares the activities of different noble metal catalysts. The activity of the synthesized catalysts is higher or close to other Ag catalysts and even comparable with some Pd- or Pt-based catalysts [34–38].

**Table 3.** The activity of noble metal catalysts in reduction of nitroarenes with $NaBH_4$.

| Catalysts | t (min) | k ($min^{-1}$) | Ref. |
|---|---|---|---|
| Ag/$CeO_2$ (red) | 6 | 0.465 | This work |
| Ag-$CeO_2$ | 11 | 0.232 | This work |
| Ag/$CeO_2$ | 8 | 0.656 | This work |
| Ag@BCN | 6 | 0.196 | [34] |
| AgNPs/PAN | 70 | 0.046 | [35] |
| Ag@$CeO_2$ | 7 | 0.32 | [36] |
| Ag@$CeO_2$ | - | 1.96 | [37] |
| Pd/C (commercial) | 6 | 0.77 | [38] |
| Pt/C | 30 | 0.058 | [38] |
| Pd/$Fe_2O_3$ | 5 | 0.359 | [38] |

## 3. Discussion

We found that the prepared silver-based catalysts exhibited different activity in the p-nitrophenol reduction under ambient conditions in accordance with the effects of the preparation method that affected the oxidation state of silver and the size of metal particles, their dispersion on the surface or within the catalyst, and interaction with the ceria support.

The Ag–$CeO_2$ prepared by the co-precipitation method is characterized by the formation of spherical agglomerates. The XRD data shows that both small and large metallic Ag particles are formed in this catalyst, owing to the redox reaction between silver and ceria precursors during the co-precipitation. This catalyst showed the lowest activity. According to Ref. [15], the activity of silver-based catalysts in nitrophenol reduction is mainly determined by silver active sites dispersed on the catalyst surface. Accordingly, we can assume that the relatively low activity of the Ag–$CeO_2$ catalyst is connected with the Ag distribution both on the surface and inside the agglomerates, and only a part of silver is accessible for the reaction. Additionally, the dispersion of silver should be considered, and the high amount of relatively large silver particles in Ag–$CeO_2$ leads to a decreased active surface of silver and, therefore, to low activity.

The catalysts prepared by the impregnation techniques, especially for Ag/$CeO_2$, are characterized by higher activity than the co-precipitated one. TEM and XRD data show that silver is stabilized predominantly in a highly dispersed form, i.e., the active surface of silver is higher than that for Ag–$CeO_2$ catalyst. In the TPR profiles, the increased intensity of the low-temperature peaks for the catalysts prepared by impregnation indicates that silver is well dispersed, likely present as silver oxide and/or as mixed silver-cerium oxide species, and it is in good contact with the ceria surface. The area of these peaks is connected with the amount of easily reducible silver oxide-like species. It is expected that the reduction of this oxidized silver species by $NaBH_4$ occurs during the catalytic reaction with the formation of highly active metallic silver species well interacting with ceria surface. The highest amount of this species for Ag/$CeO_2$ catalyst correlates with the highest activity of this catalyst.

As for the Ag/$CeO_2$(red), the additional reductive pretreatment of ceria support before the impregnation leads to the partial reduction of silver during the impregnation and formation of relatively large silver particles. This explains the lower activity of the Ag/$CeO_2$(red) catalyst as compared to the one of Ag/$CeO_2$. Thus, the activity of Ag/$CeO_2$ catalysts is mainly determined by the active surface of silver, and Ag stabilization in a highly dispersed state appears favorable when Ag was deposited by the classical impregnation technique that resulted suitable for the preparation of Ag/$CeO_2$ catalyst with high activity in the p-nitrophenol reduction.

## 4. Materials and Methods

### *4.1. Synthesis of Catalysts*

Ceria-based catalysts were prepared by two methods: precipitation [25,39] and impregnation [40]. The Ag–$CeO_2$ catalyst was prepared by co-precipitation method using mixed aqueous solution of $AgNO_3$ (2.1 g) and $Ce(NO_3)_3{\cdot}6H_2O$ (21.8 g), where the diluted ammonia solution (11.6 mL of 25% $NH_4OH$ solution diluted with 36.2 ml of $H_2O$) was added at room temperature immediately with a rotary stirrer (350 rpm). Stirring for 1 min was used, then the co-precipitate was evenly heated by steam for 10 min in an autoclave at 120 °C. The co-precipitate was centrifuged, washed by distilled water, dried overnight at 120 °C, and calcined at 500 °C for 5 h in air. The Ag loading in the synthesized catalysts was 20 mol. % (corresponding to ~13.6 wt. %). The $CeO_2$ support was synthesized by the same method via precipitation of cerium(III) nitrate hexahydrate with ammonia solution.

Two Ag/$CeO_2$ catalysts with Ag loading of 20 mol. % were synthesized with impregnation techniques using ceria prepared by precipitation and calcined at 500 °C for 5h. The as-prepared ceria or the one pre-reduced at a temperature of 500 °C for 30 min in $H_2$/Ar flow (10 vol. % $H_2$) were impregnated with an $AgNO_3$ aqueous solution. Then the samples were dried at 120 °C overnight and calcined at 500 °C for 1 h. The catalysts were denoted as Ag/$CeO_2$ (as-prepared ceria as a support) and Ag/$CeO_{2(red)}$ (pre-reduced ceria as support), respectively. The reductive pretreatment of ceria support yields surface $Ce^{3+}$ species. The subsequent impregnation with $AgNO_3$ results in the redox reaction between $Ce^{3+}{}_{sur.}$ and $Ag^{+}{}_{aq.}$ to yield $Ce^{4+}$ and Ag, and the enhanced interfacial Ag–$CeO_2$ interaction [16]. The $Ce^{3+}$ and $Ag(NH_3)^{2+}$ ions participate in the same redox reaction during the co-precipitation of the corresponding nitrates by ammonia solution.

### *4.2. Materials Characterization*

The porous structures of the obtained materials were investigated using the low-temperature $N_2$ adsorption (−196 °C) at an automatic gas adsorption analyzer TriStar 3020 (Micromeritics, Norcross, GA, USA). The multipoint BET method using the flattening of the adsorption isotherms (the $p/p_0$ range was from 0.05 to 0.30) was applied to calculate specific surface area ($S_{BET}$). The BJH-Desorption method accompanied by the analysis of the desorption branches of the $N_2$ adsorption–desorption isotherms was employed to estimate the pore size distributions. Prior to the experiments, the degassing of the samples (50–80 mg) at 200 °C and 100 mtorr for 2 h was used.

The powder X-ray diffraction (XRD) analysis was carried out on the Miniflex 600 diffractometer Riguku (Austin, TX, USA) with $CuK_\alpha$ radiation (λ = 1.5418 Å) equipped with a monochromator to study the phase composition of the prepared materials. The scanning rate was 0.2 deg/min, and the 2Θ range was 2–90°. The PCPDFWIN databases and the full-profile analysis program POWDER CELL 2.4 were used. The coherent scattering region (CSR) and Scherrer equation were used to estimate the particle sizes.

The electron microscope JEM-2200 FS (JEOL, Tokyo, Japan) was applied to investigate the sample structure with the high-resolution transmission electron microscopy (HR TEM). The resolution was 0.1 nm, the accelerating voltage was 200 kV. The DigMicrograph (GATAN) software allowed determining the crystal lattice parameters by applying the Fourier transform.

The temperature-programmed reduction in hydrogen ($H_2$-TPR) on the chemisorption analyzer ChemiSorb 2750 (Micromeritics, Norcross, GA, USA) made it possible to study the features of the sample reduction. The thermal conductivity detector (TCD signal) was used. The heating rate was 10°/min, the flow comprised an argon–hydrogen mixture (10 vol. % $H_2$). The flow rate was 20 mL/min.

### *4.3. Catalytic Activity Test*

The room-temperature (25 °C) p-nitrophenol reduction with $NaBH_4$ was used to study the catalytic properties of the prepared materials in aqueous media and at atmospheric pressure. Firstly, 28.9 mg of $NaBH_4$ were added into 50 mL of aqueous solution of p-nitrophenol (0.15 mmol/L) under rapid magnetic stirring to produce a homogeneous solution. The stirring rate was 700 rpm and it was previously optimized to carry out the reaction under these conditions in a kinetic mode. Then 6 mg of the as-synthesized catalyst was added to the mixture under stirring. The yellow color of the solution was due to the light absorption by p-nitrophenolate ion (maximum at 400 nm). The ion was formed through the p-nitrophenol dissociation under basic conditions. During the catalytic experiments, the color change from bright yellow to colorless was observed due to the p-nitrophenolate conversion into p-aminophenol. The spectrometer Solar PB 60 was used to measure the UV-Vis spectra and control the reaction progress.

## 5. Conclusions

Herein, the effect of the preparation method on the activity of Ag–$CeO_2$ catalysts in the room-temperature p-nitrophenol reduction was shown. The co-precipitation of Ag and Ce nitrates by ammonia yielded Ag–$CeO_2$ agglomerates with sizes of ~400 nm consisting of aggregated metallic Ag and $CeO_2$ particles with size ranging from few nm to 5–20 nm. The activity of this catalyst is relatively low due to the distribution of silver particles both inside the agglomerates and on the catalyst surface. The impregnation technique was favorable for the preparation of oxidized Ag species well dispersed on the ceria surface with high activity in the p-nitrophenol reduction. This finding was associated with the formation of active metallic silver nanoparticles homogeneously distributed on the external surface of ceria during the catalytic reaction. The pre-reduction of ceria support before impregnation did not lead to increased activity because of the formation of large and less active silver particles due to the redox reaction between $Ag^+{}_{aq}$ ions with $Ce^{3+}{}_{sur}$ species.

In conclusion, the $Ag/CeO_2$ catalyst prepared by impregnation technique is characterized by high activity in p-nitrophenol reduction (the first-order rate constant k = 0.656 $min^{-1}$) in aqueous media and may be explored as cheaper counterparts of Pt or Pd catalysts.

**Author Contributions:** M.C.: investigation (synthesis, characterization, catalytic tests), writing—original draft preparation; N.M.: methodology, investigation (characterization), writing—review and editing; V.Z.: TEM studies, writing—original draft preparation (TEM); M.S.: methodology, writing—review and editing; L.F.L.: writing—review and editing; G.M.: conceptualization, writing—review and editing, supervision, project administration, funding acquisition. All authors have read and agreed to the published version of the manuscript.

**Funding:** This research was funded by RUSSIAN SCIENCE FOUNDATION, grant number 18-73-10109.

**Conflicts of Interest:** The authors declare no conflict of interest.

## References

1. Bamba, D.; Coulibaly, M.; Robert, D. Nitrogen-containing organic compounds: Origins, toxicity and conditions of their photocatalytic mineralization over $TiO_2$. *Sci. Total Environ.* **2017**, *580*, 1489–1504. [CrossRef] [PubMed]
2. Gil, J.; Ferreira, L.F.; Silva, V.C.; Oliveira, A.C.; De Oliveira, R.R.; Jacinto, M.J. Facile fabrication of functionalized core-shell $Fe_3O_4$@$SiO_2$@Pd microspheres by urea-assisted hydrothermal route and their application in the reduction of nitro compounds. *Environ. Nanotechnol. Monit. Manag.* **2019**, *11*, 100220. [CrossRef]
3. Peres, C.M.; Agathos, S.N. Biodegradation of nitroaromatic pollutants: From pathways to remediation. *Biotechnol. Ann. Rev.* **2010**, *6*, 197–220.
4. Xiao-Qiong, W.; Xing-Wen, W.; Qing, H.; Jiang-Shan, S.; Hong-Wu, Z. In situ synthesized gold nanoparticles in hydrogels for catalytic reduction of nitroaromatic compounds. *Appl. Surf. Sci.* **2015**, *331*, 210–218.
5. Pan, T.; Chen, B. Facile fabrication of Shewanella@graphene core-shell material and its enhanced performance in nitrobenzene reduction. *Sci. Total Environ.* **2018**, *658*, 324–332. [CrossRef]
6. Nezamzadeh-Ejhieh, A.; Khorsandi, S. Photocatalytic degradation of 4-nitrophenol with ZnO supported nano-clinoptilolite zeolite. *J. Ind. Eng. Chem.* **2013**, *20*, 937–946. [CrossRef]
7. Jiang, P.; Zhou, J.; Zhang, A.; Zhong, Y. Electrochemical degradation of p-nitrophenol with different processes. *J. Environ. Sci.* **2010**, *22*, 500–506. [CrossRef]
8. Begum, R.; Rehan, R.; Farooqi, H.Z.; Butt, Z.; Ashraf, S. Physical chemistry of catalytic reduction of nitroarenes using various nanocatalytic systems: Past, present, and future. *J. Nanopart. Res.* **2016**, *18*, 231–255. [CrossRef]
9. Guzman, M.; Estrada, M.; Miridonov, S.; Simakov, A. Synthesis of cerium oxide (IV) hollow nanospheres with tunable structure and their performance in the 4-nitrophenol adsorption. *Microporous Mesoporous Mater.* **2019**, *278*, 241–250. [CrossRef]
10. Yang, B.; Qi, Y.; Liu, R. Pilot-Scale Production, Properties and Application of Fe/Cu Catalytic-Ceramic-Filler for Nitrobenzene Compounds Wastewater Treatment. *Catalysts* **2019**, *9*, 11. [CrossRef]
11. Song, J.; Huang, Z.-F.; Pan, L.; Li, K.; Zhang, X.; Wang, L.; Zou, J.-J. Review on selective hydrogenation of nitroarene by catalytic, photocatalytic and electrocatalytic reactions. *Appl. Catal. B* **2018**, *227*, 386–408. [CrossRef]
12. Shimizu, K.; Miyamoto, Y.; Satsuma, A. Size- and support-dependent silver cluster catalysis for chemoselective hydrogenation of nitroaromatics. *J. Catal.* **2010**, *270*, 86–94. [CrossRef]
13. Mittal, M.; Gupta, A.; Pandey, O.P. Role of oxygen vacancies in Ag/Au doped $CeO_2$ nanoparticles for fast photocatalysis. *Sol. Energy* **2018**, *165*, 206–216. [CrossRef]
14. Patra, A.K.; Vo, N.T.; Kim, D. Highly robust magnetically recoverable $Ag/Fe_2O_3$ nanocatalyst for chemoselective hydrogenation of nitroarenes in water. *Appl. Catal. A Gen.* **2017**, *538*, 148–156. [CrossRef]
15. Liao, G.; Gong, Y.; Zhong, L.; Fang, J.; Zhang, L.; Xu, Z.; Gao, H.; Fang, B. Unlocking the door to highly efficient Ag-based nanoparticles catalysts for $NaBH_4$-assisted nitrophenol reduction. *Nanoresearch* **2019**, *12*, 2407–2436. [CrossRef]
16. Grabchenko, M.V.; Mamontov, G.V.; Zaikovskii, V.I.; La Parola, V.; Liotta, L.F.; Vodyankina, O.V. The role of metal–support interaction in $Ag/CeO_2$ catalysts for CO and soot oxidation. *Appl. Catal. B* **2020**, *260*, 118148. [CrossRef]

17. Tao, L.; Shi, Y.; Huang, Y.-C.; Chen, R.; Zhang, Y.; Huo, J.; Zou, Y.; Yu, G.; Luo, J.; Dong, C.-L.; et al. Interface Engineering of Pt and $CeO_2$ Nanorods with Unique Interaction for Methanol Oxidation. *Nano Energy* **2018**, *53*, 604–612. [CrossRef]
18. Hossain, S.T.; Azeeva, E.; Zhang, K.; Zell, E.T.; Bernard, D.T.; Balaz, S.; Wang, R. A comparative study of CO oxidation over Cu-O-Ce solid solutions and $CuO/CeO_2$ nanorods catalysts. *Appl. Surf. Sci.* **2018**, *455*, 132–143. [CrossRef]
19. Zhang, S.; Xia, Z.; Ni, T.; Zhang, Z.; Ma, Y.; Qu, Y. Strong electronic metal-support interaction of $Pt/CeO_2$ enables efficient and selective hydrogenation of quinolines at room temperature. *J. Catal.* **2018**, *359*, 101–111. [CrossRef]
20. Verma, P.; Kuwahara, Y.; Mori, K.; Yamashita, H. Plasmonic catalysis of Ag nanoparticles deposited on CeO2 modified mesoporous silica for the nitrostyrene reduction under light irradiation conditions. *Catal. Today* **2018**, *324*, 83–89. [CrossRef]
21. Golubina, E.V.; Lokteva, E.S.; Erokhin, A.V.; Veligzhanin, A.A.; Zubavichus, Y.V.; Likholobov, V.A.; Lunin, V.V. The role of metal–support interaction in catalytic activity of nanodiamond-supported nickel in selective phenylacetylene hydrogenation. *J. Catal.* **2016**, *344*, 90–99. [CrossRef]
22. Fiorenza, R.; Spitaleri, L.; Gulino, A.; Sciré, S. High-Performing Au-Ag Bimetallic Catalysts Supported on Macro-Mesoporous $CeO_2$ for Preferential Oxidation of CO in $H_2$-Rich Gases. *Catalysts* **2020**, *10*, 49. [CrossRef]
23. Grabchenko, M.V.; Mikheeva, N.N.; Mamontov, G.V.; Salaev, M.A.; Liotta, L.F.; Vodyankina, O.V. $Ag/CeO_2$ Composites for Catalytic Abatement of CO, Soot and VOCs. *Catalysts* **2018**, *8*, 285. [CrossRef]
24. Thommes, M.; Kaneko, K.; Neimark, A.V.; Olivier, J.P.; Rodriguez-Reinoso, F.; Rouquerol, J.; Sing, K.S. Physisorption of gases, with special reference to the evaluation of surface area and pore size distribution (IUPAC Technical Report). *Pure Appl. Chem.* **2015**, *87*, 1051–1069. [CrossRef]
25. Yamazaki, K.; Kayama, T.; Dong, F.; Shinjoh, H. A mechanistic study on soot oxidation over $CeO_2$-Ag catalyst with 'rice-ball' morphology. *J. Catal.* **2011**, *282*, 289–298. [CrossRef]
26. Montini, T.; Melchionna, M.; Monai, M.; Fornasiero, P. Fundamentals and Catalytic Applications of $CeO_2$-Based Materials. *Chem. Rev.* **2016**, *116*, 5987–6041. [CrossRef] [PubMed]
27. Mamontov, G.V.; Grabchenko, M.V.; Sobolev, V.I.; Zaikovskii, V.I.; Vodyankina, O.V. Ethanol dehydrogenation over $Ag\text{-}CeO_2/SiO_2$ catalyst: Role of $Ag\text{-}CeO_2$ interface. *Appl. Catal. A* **2016**, *528*, 161–167. [CrossRef]
28. Kim, M.J.; Han, G.-H.; Lee, S.H.; Jung, H.W.; Choung, J.W.; Kim, C.H.; Lee, K.-Y. $CeO_2$ promoted $Ag/TiO_2$ catalyst for soot oxidation with improved active oxygen generation and delivery abilities. *J. Hazard. Mater.* **2020**, *384*, 121341. [CrossRef]
29. Dutov, V.V.; Mamontov, G.V.; Zaikovskii, V.I.; Liotta, L.F.; Vodyankina, O.V. Low-temperature CO oxidation over $Ag/SiO_2$ catalysts: Effect of OH/Ag ratio. *Appl. Catal. B* **2018**, *221*, 598–609. [CrossRef]
30. Grabchenko, M.V.; Mamontov, G.V.; Zaikovskii, V.I.; La Parola, V.; Liotta, L.F.; Vodyankina, O.V. Design of Ag $CeO_2/SiO_2$ catalyst for oxidative dehydrogenation of ethanol: Control of $Ag–CeO_2$ interfacial interaction. *Catal. Today* **2019**, *333*, 2–9. [CrossRef]
31. Sadlivskaya, M.V.; Mikheeva, N.N.; Zaikovskii, V.I.; Mamontov, G.V. Influence of Preparation Method of $Ag–CeO_2$ Catalysts on Their Structure and Activity in Soot Combustion. *Kinet. Catal.* **2019**, *60*, 432–438. [CrossRef]
32. Fu, Y.; Xu, P.; Huang, D.; Zeng, G.; Lai, C.; Qin, L.; Li, B.; He, J.; Yi, H.; Cheng, M.; et al. Au nanoparticles decorated on activated coke via a facile preparation for efficient catalytic reduction of nitrophenols and azo dyes. *Appl. Surf. Sci.* **2019**, *473*, 578–588. [CrossRef]
33. Zhao, P.; Feng, X.; Huang, D.; Yang, G.; Astruc, D. Basic concepts and recent advances in nitrophenol reduction by gold- and other transition metal nanoparticles. *Coord. Chem. Rev.* **2015**, *287*, 114–136. [CrossRef]
34. Qiu, X.; Liu, Q.; Song, M.X.; Huang, C. Hydrogenation of nitroarenes into aromatic amines over Ag@BCN colloidal catalysts. *J. Colloid Interface Sci.* **2016**, *447*, 131–137. [CrossRef] [PubMed]
35. Liu, Y.; Jiang, G.; Li, L.; Chen, H.; Huang, Q.; Jiang, T.; Du, X. Silver nanoparticles supported on electrospun polyacrylonitrile nanofibrous mats for catalytic applications. *MRS Commun.* **2016**, *6*, 31–40. [CrossRef]
36. Wang, Y.-Y.; Shu, Y.; Xu, J.; Pang, H. Facile one-step synthesis of $Ag@CeO_2$ core–shell nanospheres with efficient catalytic activity for the reduction of 4-nitrophenol. *CrystEngComm.* **2017**, *19*, 684–689. [CrossRef]

37. Shi, Y.; Zhang, X.L.; Zhu, Y.M.; Tan, H.L.; Chen, X.S.; Lu, Z.H. Core–shell structured nanocomposites Ag@$CeO_2$ as catalysts for hydrogenation of 4-nitrophenol and 2-nitroaniline. *RSC Adv.* **2016**, *6*, 47966–47973. [CrossRef]
38. Jiang, S.-F.; Ling, L.-L.; Xu, Z.; Liu, W.-J.; Jiang, H. Enhancing the Catalytic Activity and Stability of Noble Metal Nanoparticles by the Strong Interaction of Magnetic Biochar Support. *Ind. Eng. Chem. Res.* **2018**, *57*, 13055–13064. [CrossRef]
39. Deng, X.; Li, M.; Zhang, J.; Hu, X.; Zheng, J.; Zhang, N.; Chen, B.H. Constructing nano-structure on silver/ceria-zirconia towards highly active and stable catalyst for soot oxidation. *Chem. Eng. J.* **2017**, *313*, 544–555. [CrossRef]
40. Grabchenko, M.V.; Mamontov, G.V.; Zaikovskii, V.I.; Vodyankina, O.V. Effect of the metal−support interaction in Ag/$CeO_2$ catalysts on their activity in ethanol oxidation. *Kinet. Catal.* **2017**, *58*, 642–648. [CrossRef]